

X-RAY OPTICS

https://doi.org/10.1070/QEL18048

The concept of a stigmatic flat-field X-ray spectrograph based on conical diffraction

A.O. Kolesnikov, E.N. Ragozin, A.N. Shatokhin

Abstract. **The optical scheme of a flat-field stigmatic X-ray spectrograph, which includes a grazing-incidence focusing mirror and a concave fan-type diffraction grating crossed with respect to the mirror and mounted in a conical diffraction scheme, is calculated analytically. Spectral images of a point monochromatic source are obtained by numerical ray tracing, confirming the high quality of spectral images at a level of 1 × 4 μm. It is assumed that the use of small grazing incidence angles in combination with the application of multilayer reflective coatings, including aperiodic ones, will make it possible to extend the working spectral range of the stigmatic spectrograph to the region of the 'tender' ($\hbar\omega \approx 1.5 - 6$ keV) X-ray range.**

Keywords: *tender X-ray range, conical diffraction, fan grating, flat field, stigmatism.*

1. Introduction

Recent years have seen the advent of new sources of X-ray radiation with unique properties [high instantaneous (pulsed) brightness and spatial coherence, small size] excited by multiterawatt/subpetawatt femtosecond lasers. Among these sources are the high harmonics of laser radiation with a photon energy of several hundred electronvolts [1], BISER (Burst Intensification by Singularity Emitting Radiation) [2, 3], a beam of betatron (synchrotron) radiation [4 – 6], which is produced by transverse oscillations of accelerated electrons. Mention should also be made of sources based on the bremsstrahlung of a beam of laser-accelerated electrons and the characteristic radiation excited by the electrons in a converter target [7, 8]. These new sources stimulate the development of new optical-spectral instruments for their study and characterisation, and invite the development of tools for manipulating soft, tender ($\hbar\omega \approx 1.5 - 6$ keV) and hard X-ray beams (resolution into a spectrum, monochromatisation, focusing, and beam splitting).

In the design of a flat-field stigmatic X-ray spectrograph (with a focal surface, which the spectrum is displayed on, that is well approximated by a plane and therefore compatible with modern CCD detectors), we turned to cone diffraction [9] due to its high energy efficiency [10]. In recent years, considerable attention has been given to conical diffraction and the development of a technology for manufacturing gratings suitable for operation in the conical diffraction scheme (see, for example, Refs [11, 12]). Furthermore, attempts to advance the short-wavelength boundary of the flat field to the region of wavelengths shorter than $\lambda \sim 10$ Å with a spherical VLS grating (varied line-space grating; a grating in which the spacing is a monotonic function of the coordinate on the aperture) in the in-plane mount run into difficulties, while the flat focal field is the immanent property of conical diffraction. In the conical diffraction mount, radiation is incident on a diffraction grating (DG) along the direction of the grooves. In this case, the shading effect is completely absent even at very small angles of grazing incidence, in contrast to the classical scheme (in-plane mount) with the source placed near the principal plane (Fig. 1). One would also expect that the efficiency of a multilayer interference reflective coating in the conical diffraction scheme will be close to the efficiency of 'ordinary' multilayer X-ray mirrors, because in this case the angle between the incident ray and the local normal to the groove profile changes insignificantly along the groove profile. This will make it possible to develop flat-field diffraction spectrometers not only in the soft and 'tender', but also in the hard X-ray range. It has been demonstrated, in particular, that multilayer X-ray mirrors are capable of reflecting radiation at least up to 69 (W/Si) and 90 keV (Ni/C) [13, 14]. It is pertinent to note that the use of multilayer reflective coatings has shown its effectiveness in relation to plane gratings with 'blaze' [15] and spherical VLS gratings [16] operating in the classical (in-plane) mount at grazing incidence of radiation. It is also assumed that multilayer grazing-incidence mirrors, including aperiodic/stack multilayer mirrors, can be used to focus the hard ($E \approx 10 - 12$ keV) radiation from a Compton backscattering X-ray source [17].

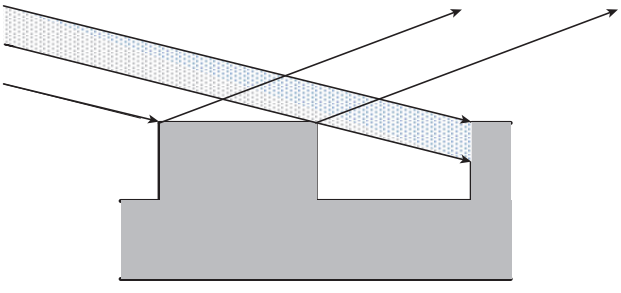

Figure 1. Effect of shading during oblique (grazing) beam incidence on the DG in the in-plane mount scheme.

A.O. Kolesnikov, E.N. Ragozin, A.N. Shatokhin P.N. Lebedev Physical Institute of the Russian Academy of Sciences, Leninsky prosp. 53, 119991 Moscow, Russia; e-mail: enragozin@gmail.com

Received 16 December 2021
Kvantovaya Elektronika **52** (5) 491–496 (2022)
Translated by E.N. Ragozin

The purpose of this work is to formulate the design principle (concept) of a stigmatic flat field X-ray spectrograph based on conical diffraction and to demonstrate the possibilities of the scheme by the example of a four-meter long spectrograph, in which the short-wavelength limit of the working spectral range lies in the tender X-ray range, in the wavelength range of 2 – 8 Å.

2. Concave diffraction grating in the conical diffraction mount

The scheme of the spectrograph outwardly resembles the Kirkpatrick – Baez scheme, which includes two crossed concave grazing-incidence mirrors that focus radiation in two perpendicular directions [18] (Fig. 2a). However, instead of the second mirror, the spectrograph uses a fan-type concave DG*, which forms spectral images of the source in a plane perpendicular to the tangent to the central DG groove (Fig. 2b), and therefore the instrument is a flat-field spectrograph. The mirror focuses the beam of rays coming from the source in the horizontal direction, and the concave DG focuses the beam in the vertical direction and performs its spatial decomposition into a spectrum in the horizontal direction (along a circular arc in the vertical plane). As shown below, with an appropriate choice of configuration parameters, the spectral images of a point tender X-ray source have a size of only a few micrometres, which makes it possible to classify the spectrograph as a stigmatic one.

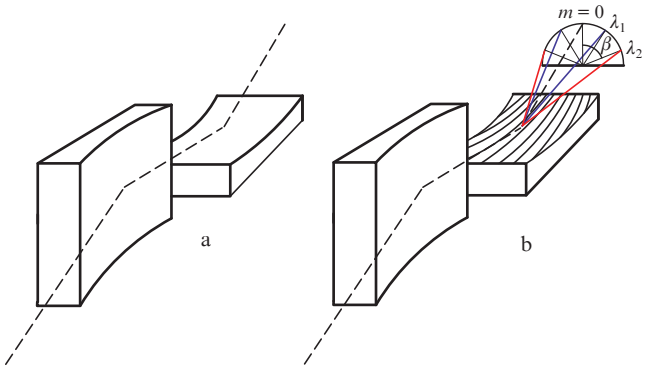

Figure 2. Configurations of (a) a Kirkpatrick – Baez microscope and (b) a stigmatic flat-field X-ray spectrograph based on conical diffraction. The spectrograph elements are a grazing-incidence focusing mirror and a fan-type concave diffraction grating mounted in the grazing-incidence conical diffraction scheme ($\lambda_2 > \lambda_1$).

As is well known (see, for example, Ref. [19]), in the general case (the central ray of the incident beam does not necessarily lie in the principal plane) the DG equation (Fig. 3) is of the form

$$\sin\theta(\sin\alpha + \sin\beta) = mp\lambda, \qquad (1)$$

where θ is the angle that the ray AO incident on the DG makes with the tangent to its central groove (the z axis); α and β are the angles between the x axis and the projections onto the principal xy plane of the rays AO and OB, respectively; p is the frequency of DG grooves; and m is the diffraction order. The angle θ' that the diffracting ray makes with the tangent to the central groove is equal to θ so that all diffracting rays are the generatrices of the cone with an opening angle of 2θ whose axis coincides with this tangent (hence the name: conical diffraction). The spectrum is located on a circle of radius $L\sin\theta$, where L is the distance from the DG centre to the focal plane (detector plane).

To design the scheme of a stigmatic spectrograph, we need to derive equations describing the position of the horizontal (spectral) and vertical foci. To do this, we employ, as usual, Fermat's principle, which requires the construction of the optical path function.

Let us place the origin O of the rectangular coordinate system at the centre of the grating of radius R (see Fig. 3). The x axis is directed along the normal to the grating, the z axis is directed along the tangent to its central groove at point O, and the y axis is at an angle of 90° to the central groove along the tangent to the grating surface at the origin. In spherical coordinates, the position of a point source (denoted by point A) will have coordinates (r, θ, α), where r is the distance from the beam focus to the origin of coordinates; θ is the angle between the central ray AO of the incident beam and the z axis (conical angle); and α is the angle between the projection of the ray AO on the principal plane xy and the x axis. The projection of the wave vector of the incident beam onto the z axis is positive. Point P is an arbitrary point on a grating groove (it is assumed that the grating grooves are infinitely thin lines). The actual shape of the groove is important for the intensity distribution in the spectrum, but does not affect the focusing properties of the grating. In doing so, we assume that $R\sin\theta$, r, and r' are much longer than the grating aperture.

The position of the source is given by the vector $(r\sin\theta\cos\alpha, r\sin\theta\sin\alpha, r\cos\theta)$, and the position of the source image, of point B, by the vector $(r'\sin\theta'\cos\beta,\ r'\sin\theta'\sin\beta,\ r'\cos\theta')$. The position of point P can be described by the vector $(x(y, z), y, z)$, and $x(y, z) = R - \sqrt{R^2 - y^2 - z^2} \approx (y^2 + z^2)/(2R)$.

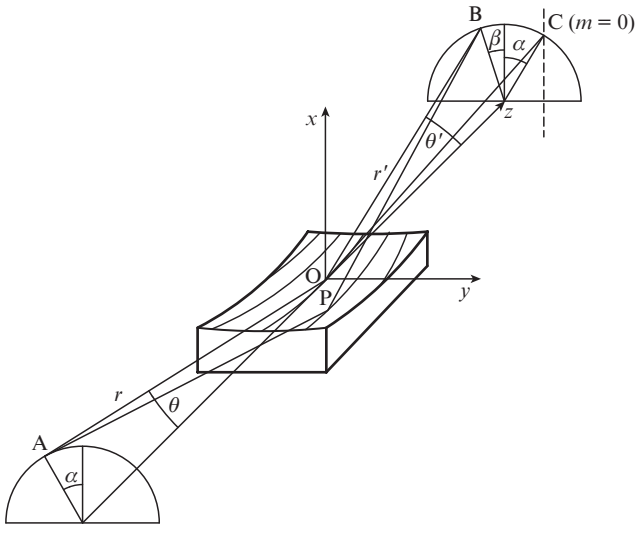

Figure 3. Fan spherical DG of radius R in the conical diffraction scheme: A is a point source, B is its spectral image, and P is an arbitrary point on a grating groove.

*The grooves (lines) of a plane fan grating converge at one point. In the case of a spherical fan grating, the projections of lines on a plane tangent to the sphere at the centre of the grating converge at one point.

We calculate the optical path function $F = \mathrm{AP} + \mathrm{PB}$ by performing expansion that takes into account the smallness of y and z in comparison with r, r' and $R\sin\theta$, with retention of the terms of the first and second order of smallness:

$$\mathrm{AP} = \left[\left(r\sin\theta\cos\alpha - \frac{y^2+z^2}{2R}\right)^2 + (r\sin\theta\sin\alpha - y)^2 + (r\cos\theta - z)^2\right]^{1/2} \approx r - y\sin\theta\sin\alpha + \frac{y^2}{2}\left(\frac{1-\sin^2\theta\sin^2\alpha}{r} - \frac{\sin\theta\cos\alpha}{R}\right) - z\cos\theta + \frac{z^2}{2}\left(\frac{\sin^2\theta}{r} - \frac{\sin\theta\cos\alpha}{R}\right) - yz\frac{\sin\theta\cos\theta\sin\alpha}{r}. \quad (2)$$

Similarly,

$$\mathrm{PB} = \left[\left(r'\sin\theta'\cos\beta - \frac{y^2+z^2}{2R}\right)^2 + (r'\sin\theta'\sin\beta - y)^2 + (r'\cos\theta' - z)^2\right]^{1/2} \approx r' - y\sin\theta'\sin\beta + \frac{y^2}{2}\left(\frac{1-\sin^2\theta'\sin^2\beta}{r'} - \frac{\sin\theta'\cos\beta}{R}\right) - z\cos\theta' + \frac{z^2}{2}\left(\frac{\sin^2\theta'}{r'} - \frac{\sin\theta'\cos\beta}{R}\right) - yz\frac{\cos\theta'\sin\theta'\sin\beta}{r'}. \quad (3)$$

The optical length F of the path passing through the point P with coordinates $(x(y, z), y, z)$ is described by the expression:

$$F = \mathrm{AP} + \mathrm{PB} = r + r' - y(\sin\theta\sin\alpha + \sin\theta'\sin\beta) + \frac{y^2}{2} \times \left(\frac{1-\sin^2\theta\sin^2\alpha}{r} - \frac{\sin\theta\cos\alpha}{R} + \frac{1-\sin^2\theta'\sin^2\beta}{r'} - \frac{\sin\theta'\cos\beta}{R}\right) - z(\cos\theta + \cos\theta') + \frac{z^2}{2}\left(\frac{\sin^2\theta}{r} - \frac{\sin\theta\cos\alpha}{R} + \frac{\sin^2\theta'}{r'} - \frac{\sin\theta'\cos\beta}{R}\right) - yz\left(\frac{\cos\theta\sin\theta\sin\alpha}{r} + \frac{\cos\theta'\sin\theta'\sin\beta}{r'}\right). \quad (4)$$

Let $N = 0$ be the number of the central groove and the groove number $N(y, z)$ be defined by the 2D polynomial

$$N(y, z) = N_{10}y + N_{01}z + N_{20}y^2 + N_{02}z^2 + N_{11}yz + \ldots. \quad (5)$$

The meaning of the coefficients N_{ij}: N_{10} is the spatial groove frequency, N_{11} specifies the fanning (convergence and divergence of grooves), N_{02} specifies the curvature of the grooves, N_{20} is the gradient of the groove frequency in the direction of the y axis, and $N_{01} = 0$, because the groove number cannot change when moving point P from point O along the z axis, since the z axis is tangent to the central groove owing to the choice of the coordinate system.

In order for point B to be the spectral image of point A at a wavelength λ in diffraction order m, it is necessary that the optical path changes exactly by $m\lambda$ when point P moves from the groove with number N to the groove with number $N + 1$, i.e., it is necessary that the following equalities should be fulfilled:

$$\frac{\partial F}{\partial y} = m\lambda\frac{\partial N}{\partial y}, \quad \frac{\partial F}{\partial z} = m\lambda\frac{\partial N}{\partial z}. \quad (6)$$

Substituting expressions (4) and (5) into Eqns (6) and bringing the terms of equal (zero and first) power in the y and z coordinates, we obtain

$$y^0, z^0: \begin{cases} -\sin\theta\sin\alpha - \sin\theta'\sin\beta = m\lambda N_{10}, \\ -\cos\theta - \cos\theta' = m\lambda N_{01} = 0; \end{cases}$$

$$y^1, z^1: \begin{cases} y\left(\frac{1-\sin^2\theta\sin 2\alpha}{r} - \frac{\sin\theta\cos\alpha}{R} + \frac{1-\sin^2\theta'\sin^2\beta}{r'} - \frac{\sin\theta'\cos\beta}{R}\right) - z\left(\frac{\cos\theta\sin\theta\sin\alpha}{r} + \frac{\cos\theta'\sin\theta'\sin\beta}{r'}\right) \\ = m\lambda(2N_{20}y + N_{11}z), \\ z\left(\frac{\sin^2\theta}{r} - \frac{\sin\theta\cos\alpha}{R} + \frac{\sin^2\theta'}{r'} - \frac{\sin\theta'\cos\beta}{R}\right) \\ - y\left(\frac{\cos\theta\sin\theta\sin\alpha}{r} + \frac{\cos\theta'\sin\theta'\sin\beta}{r'}\right) \\ = m\lambda(2N_{02}z + N_{11}y). \end{cases} \quad (7)$$

It follows from the second equality (7) that $\sin\theta = \sin\theta'$, and the cosines of these angles are opposite. Then expressions (7) are rewritten as follows:

$$\begin{aligned} &-\sin\theta(\sin\alpha + \sin\beta) = m\lambda N_{10}, \\ &\cos\theta\sin\theta'\left(\frac{\sin\alpha}{r} - \frac{\sin\beta}{r'}\right) = m\lambda N_{11}, \\ &\frac{1-\sin^2\theta\sin^2\alpha}{r} + \frac{1-\sin^2\theta\sin^2\beta}{r'} \\ &-\frac{\sin\theta(\cos\alpha + \cos\beta)}{R} = 2m\lambda N_{20}, \\ &\sin^2\theta\left(\frac{1}{r} + \frac{1}{r'}\right) - \sin\theta\left(\frac{\cos\alpha + \cos\beta}{R}\right) = 2m\lambda N_{02}. \end{aligned} \quad (8)$$

The first equation is called the diffraction grating equation. The third and fourth equations define the horizontal (spectral) and vertical focal curves. The second equation specifies the required 'fanning' of the grating. In the internal diffraction order, $\sin\alpha + \sin\beta < 0$ (in the case when the y coordinate of the source is less than the y coordinate of the image), which corresponds to $m > 0$ and positive N_{10}.

From the practical point of view, as would be expected, the grating cannot transform a beam diverging in the horizontal direction into a beam converging due to the coefficient N_{20}. Therefore, an additional optical element focusing in this direction is needed: a mirror crossed with respect to the grating, as shown in Fig. 2b. Then instead of r in the third equation of system (8) it is necessary to substitute the negative value r_h, equal in absolute value to the distance from the grating to the horizontal focus of the beam incident on the grating. In the case of an incident beam converging in the horizontal (spectral) direction at $N_{20} = 0$, the spectral focal curve is practically a circle: the section of the cone by the plane $z =$ const (see Figs. 2b and 3). The coefficient N_{20} determines the rotation of the cone secant plane around the axis parallel to x and passing through the point C (see Fig. 3).

3. Scheme of the spectrograph

We pass on to the description of an example of the simplest spectrograph scheme and set $\alpha = 0$, $N_{20} = 0$, and $N_{02} = 0$. Thus, we consider a DG in which the groove frequency is constant along the direction across the grooves (along the y axis for z = const) and changes monotonically in the direction along the grooves (along the z axis), i.e., a fan grating. First of all, the grazing incidence angle should be set proceeding from the working spectral range selected. This choice is determined mainly by a compromise between the requirement for a sufficiently strong linear dispersion with acceptable dimensions of the instrument and the need to obtain sufficiently high reflection coefficients of the mirror and grating in the chosen spectral range. In this example, we will stop at a grazing angle $\theta = 1.5°$. We will revert to the issue of the efficiency of the scheme below. It is expedient to mount the grating in such a way that the 'source–grating' and 'grating–detector' distances are close, i.e., on the Rowland circle. The vertical focus therefore is $r_v = R\sin\theta/\cos\alpha = R\sin\theta$. The horizontal focus of the beam produced by the mirror should also be at the same distance after the grating. The 'angular' dispersion is defined by the expression

$$\frac{d\beta}{d\lambda} = \frac{mp}{\cos\beta\sin\theta}, \tag{9}$$

and the linear dispersion, measured along the arc of a circle of radius $R\sin^2\theta$, is given by the expression

$$\frac{ds}{d\lambda} = \frac{Rmp\sin\theta}{\cos\beta}, \tag{10}$$

where s is the length of the circular arc. For example, for a grating with $p = 2400$ mm^{-1}, $R = 80$ m, and $\theta \approx 1.5°$, for radiation with a wavelength of 10 Å in the first order of diffraction, the reciprocal linear dispersion (plate scale) is about 1.99 Å mm^{-1}. For a CCD detector with a pixel size of 13 μm, this gives 2.58×10^{-2} Å pixel^{-1}. The limiting practical spectral resolving power at this wavelength, which is limited by the spatial resolution of the detector and numerically equal to the product of the plate scale and twice the pixel size, is about 200. The theoretical resolving power of the scheme is several times higher.

The longest wavelength that can be recorded in the given example is $\lambda_{max} = \sin\theta/mp \approx 109$ Å. As λ_{max} is approached, the plate scale tends to zero. For instance, already at a wavelength of 50 Å the plate scale is $d\lambda/ds = 1.768$ Å mm^{-1} and one pixel of a CCD detector corresponds to a spectral interval of 2.3×10^{-2} Å.

When using a spherical mirror and a spherical grating, it is not possible to assemble the instrument so that the distances from the source/image to the centre of the mirror/grating are equal to $R\sin\theta$, when the aberration of meridional coma is completely absent. This can be avoided by using, for example, a slightly elliptical cylinder instead of a spherical mirror. However, below we present the results for a scheme with a spherical mirror and a spherical fan grating.

The spherical mirror and grating have the same radii of curvature $R_M = R = 80$ m. The mirror is used in the Rowland mount at a grazing incidence angle $\varphi = 1.5°$, which leads to the 'point source–mirror' distance $r_M = R_M\sin\varphi = 2094.2$ mm. The groove frequency at the grating centre is $N_{10} = 2400$ mm^{-1}, and its fanning is $N_{11} = 1.2$ mm^{-2}. The grating is located at a distance $r_{MG} = 70$ mm from the mirror. Due to the 'intervention' of the spherical surface of the grating, the focal plane is located at a distance $r_D = 2021$ mm, so that the further path length of the central ray from the mirror to the focal plane is $r_D + r_{MG} = 2091$ mm, which is ~3 mm shorter than the Rowland distance $R_M\sin\varphi$. The conical angle θ, equal to the angle of grazing incidence of the central ray on the grating, is 1.497°. Therefore, the grating is mounted in a slightly non-Rowland scheme, where the arm from the source to the grating $r_M + r_{MG} = 2164.2$ mm is ~7 cm longer than the Rowland distance $R\sin\varphi$, and the second arm r_D from the grating to the focal plane of the instrument turns out to be approximately the same 7 cm shorter that the Rowland distance. In the selected scheme, the groove convergence point (fan focus) is located on the z axis at a distance $N_{10}/N_{11} = 2400/1.2 = 2000$ mm.

Figure 4 shows the spectral images of a point monochromatic source in zero and first orders and with wavelength $\lambda = 1, 2, 3, 4, 5, 6, 7$, and 8 Å obtained by numerical ray tracing in the spectrograph scheme with the above parameters, as well as an enlarged image of a point source with a wavelength of 4 Å. One can see that the image of a monochromatic point source fits completely into a 1×4 μm cell. When using an

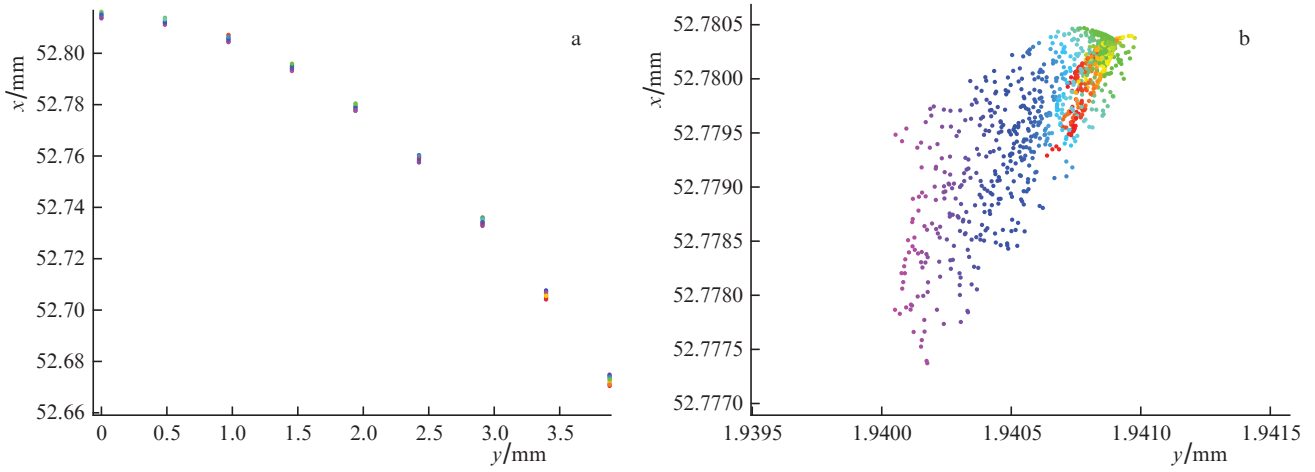

Figure 4. (Colour online) (a) Spectral images of a point monochromatic source in the zero and first diffraction orders and with wavelength $\lambda = 1, 2, 3, 4, 5, 6, 7$, and 8 Å obtained by numerical ray tracing; (b) the same for $\lambda = 4$ Å, but on a larger scale.

entrance slit parallel to the x axis (see Fig. 3), the spectral image of a monochromatic source will be a vertical (along the x axis) segment and will be approximately equal in length to the height of the illuminated section of the entrance slit in the configuration under description.

The working aperture of the mirror is 60×1.5 mm (w × h), the grating aperture is approximately 1.5×60 mm (w × l) (~3600 lines). In this case, the spectral image of the source is formed by rays from a solid angle of $\sim 5 \times 10^{-7}$ sr. The best materials for X-ray single-layer reflective coatings (Os, Au, Pt, etc.) at a grazing angle of incidence $\theta = 1.5°$ provide a conventionally acceptable reflection coefficient of more than 60% only for wavelengths exceeding 6.5 – 7.0 Å (1.9 – 1.77 keV) (Fig. 5). At a wavelength of 4 Å, a 30 nm thick gold coating provides only about 11% reflectivity, while an Os coating of the same thickness provides about 20%, which is hardly acceptable due to double reflection (mirror + grating), unless we are dealing with a directional radiation source. Therefore, single-layer reflective coatings at the specified angle of incidence can provide satisfactory reflectivity only in a small part of the tender X-ray range, which occupies the energy range $\hbar\omega \approx 1.5 – 6$ keV. Periodic multilayer mirrors (Cr/C, Os/C, etc.) provide a fairly high reflection coefficient at the maximum, but the widths of the reflectivity profiles are relatively small ($\delta\lambda_{1/2}/\lambda \sim 1/8 – 1/20$) (Figs 5 and 6).

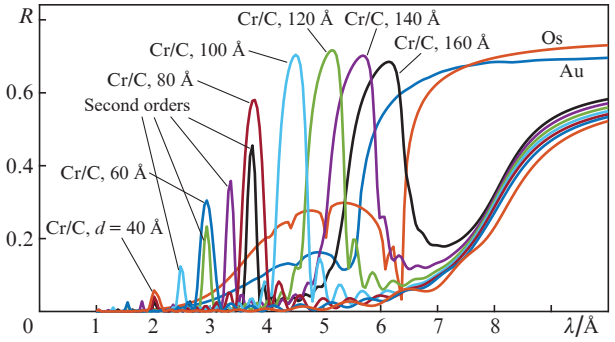

Figure 5. (Colour online) Reflection coefficients of gold and osmium coatings, as well as of Cr/C periodic multilayer mirrors with different periods d at $\theta = 1.5°$. The calculation takes into account the roughness of the grating surface (3 Å), as well as the transition layers in the multilayer structure (Cr-on-C: 6 Å; C-on-Cr: 3 Å). In all cases, the number of periods is 12, and the thickness of the Cr layer is 0.4 of the period. Along with the first-order reflection peaks, second-order interference peaks stand out in the short-wavelength part.

The problem of broadband reflection in the short-wavelength region can be solved by synthesising a multilayer coating with a period that varies along the y axis, i.e., across the direction of the grooves, as well as a similar gradient coating on the mirror. In this case, at a fixed position of the grating and mirror, the instrument will be relatively narrow-band in the short-wavelength part of the spectral operating range (1 – 5 Å). Wavelength tuning is carried out by rotating the grating around the 'fan' axis and correspondingly rotating the mirror around a horizontal axis that passes through the centre of the sphere and is perpendicular to the radius drawn from the centre of the sphere to the point of incidence of the central ray on the mirror. The Institute of Physics of Microstructures (IPM RAS, Nizhny Novgorod) has expertise

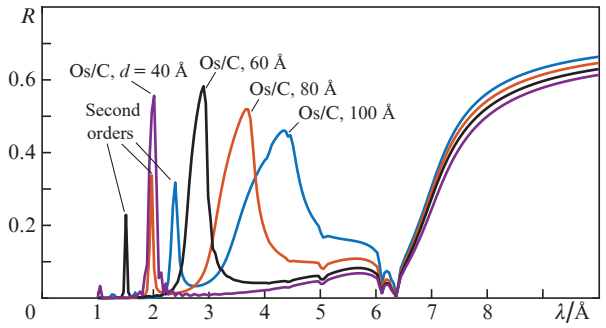

Figure 6. (Colour online) Reflection coefficients of Os/C periodic multilayer mirrors with different periods d at $\theta = 1.5°$. The calculation took into account the roughness of the grating surface (3 Å) as well as the transition layers in the multilayer structure (Os-on-C: 6 Å; C-on-Os: 3 Å). In all cases, the number of periods is 20, and the thickness of the Os layer is 0.4 of the period. Along with the first-order reflection peaks, second-order interference peaks stand out in the short-wavelength part. When constructing the plots, use was made of the optical materials constants borrowed from the website of the Centre for X-Ray Optics [20].

in synthesising multilayer mirrors with a strong period gradient across the aperture [21].

4. Conclusions

In the present work, we formulate the concept of a stigmatic flat-field high-resolution X-ray spectrograph for the region of the soft (including 'tender') X-ray range. The configuration comprises two grazing incidence optical elements: a focusing mirror and a fan-type spherical grating crossed with respect to the mirror and mounted in a conical diffraction scheme. Equations are obtained that relate the grating parameters (radius, line frequency, 'fanning', etc.) with the configuration parameters (distances, dispersion, position of the focal plane, etc.). Numerical ray tracing was used to obtain images of monochromatic point-like sources ($m\lambda = 1, 2, 3, 4, 5, 6, 7$, and 8 Å) that completely fit into a 1×4 μm pixel. Reflective coatings made of Au and Os provide satisfactory reflectivity for $\lambda > 6$ Å at a grazing angle of 1.5°. The deposition of periodic multilayer coatings based on Cr/C and Os/C with periods from 40 to 160 Å will make it possible to expand the spectral range to ~2 Å.

References

1. Preston S.G., Sanpera A., Zepf M., Blyth W.J., Smith C.G., Wark J.S., Key M.H., Burnett K., Nakai M., Neely D., Offenberger A.A. *Phys. Rev. A*, **53**, R31(R) (1996). DOI: 10.1103/PhysRevA.53.R31.
2. Pirozhkov A.S., Kando M., Esirkepov T.Zh., Gallegos P., Ahmed H., Ragozin E.N., Faenov A.Ya., Pikuz T.A., Kawachi T., Sagisaka A. *New J. Phys.*, **16**, 093003 (2014). DOI: 10.1088/1367-2630/16/9/093003.
3. Pirozhkov A.S., Esirkepov T.Zh., Pikuz T.A., Faenov A.Ya., Ogura K., Hayashi Y., Kotaki H., Ragozin E.N., Neely D., Kiriyama H., Koga J.K., Fukuda Y., Sagisaka A., Nishikino M., Imazono T., Hasegawa N., Kawachi T., Bolton P.R., Daido H., Kato Y., Kondo K., Bulanov S.V., Kando M. *Sci. Rep.*, **7**, 17968 (2017). DOI: 10.1038/s41598-017-17498-5.
4. Fourmaux S., Hallin E., Chaulagain U., Weber S., Kieffer J.C. *Opt. Express*, **28** (3), 3147 (2020). DOI: 10.1364/OE.383818.
5. Fourmaux S., Kieffer J.C., Hallin E. *Proc. SPIE*, **11036**, 110360D (2019). DOI: 10.1117/12.2523395.

6. Fourmaux S., Hallin E., Arnison P.G., Kieffer J.C. *Appl. Phys. B*, **125** (2019). DOI: 10.1007/s00340-019-7144-9.
7. Glinec Y., Faure J., Le Dain L., Darbon S., Hosokai T., Santos J.J., Lefebvre E., Rousseau J.P., Burgy F., Mercier B., Malka V. *Phys. Rev. Lett*., **94**, 025003 (2005). DOI: 10.1103/PhysRevLett.94.025003.
8. Brantov A.V., Lobok M.G., Bychenkov V.Yu. *Quantum Electron*., **47** (3), 232 (2017) [*Kvantovaya Elektron*., **47** (3), 232 (2017)]. DOI: 10.1070/QEL16302.
9. Spencer G.H., Murty M.V.R.K. *Opt. Soc. Amer*., **52**, 672 (1962).
10. Goray L., Jark W., Eichert D. *J. Synchrotron Rad*., **25**, 1683 (2018). DOI: 10.1107/S1600577518012419.
11. DeRoo C.T. PhD thes. (University of Iowa, 2016); https://doi.org/10.17077/etd.qr39wko8.
12. Goray L.I., Berezovskaya T.N., Mokhov D.V., Sharov V.A., Dashkov A.S., Pirogov E.V. *Proceedings of the XXV International Symposium 'Nanophysics and Nanoelectronics'* (Nizhny Novgorod, March 9–12, 2021) Vol. 1, pp 389, 390.
13. Joensen K.D., Gorenstein P., Christensen F.E., Hoeghoej P., Ziegler E., Susini J., Freund A.K., Wood J.L. *Proc. SPIE*, **2253**, 299 (1994). DOI: 10.1117/12.192082.
14. Joensen K.D., Gorenstein P., Wood J.L., Christensen F.E., Hoghoj P. *Proc. SPIE*, **2279**, 180 (1994). DOI: 10.1117/12.193133.
15. Senf F., Bijkerk F., Eggenstein F., Gwalt G., Huang Q., Kruijs R., Kutz O., Lemke S., Louis E., Mertin M., Packe I., Rudolph I., Schäfers F., Siewert F., Sokolov A., Sturm J.M., Waberski Ch., Wang Z., Wolf J., Zeschke T., Erko A. *Opt. Express*, **24** (12), 13220 (2016). DOI:10.1364/OE.24.013220.
16. Imazono T., Koike M., Kawachi T., Hasegawa N., Koeda M., Nagano T., Sasai H., Oue Y., Yonezawa Z., Kuramoto S., Terauchi M., Takahashi H., Handa N., Murano T., Sano K. *Appl. Opt.*, **51** (13), 2351 (2012). DOI: 10.1364/AO.51.002351.
17. Barysheva M.M., Malyshev I.V., Polkovnikov V.N., Salashchenko N.N., Svechnikov M.V., Chkhalo N.I. *Quantum Electron*., **50** (4), 401 (2020) [*Kvantovaya Elektron*., **50** (4), 401 (2020)].
18. Kirkpatrick P., Baez A.V. *J. Opt. Soc. Amer*., **38** (9), 766 (1948). DOI: 10.1364/JOSA.38.000766.
19. Werner W. *Appl. Opt*., **6** (10), 1691 (1967). DOI: 10.1364/AO.6.001691.
20. *Atomic Scattering Factor Files* (LBNL, 2021); http://henke.lbl.gov/optical_constants/.
21. Ragozin E.N., Andreev S.S., Bijkerk F., Kolachevsky N.N., Louis E., Pirozhkov A.S., Salashchenko N.N. *Proc. SPIE*, **3156**, 331 (1997). DOI: 10.1117/12.279414.